Color Appearance in Multispectral Radiosity

L. Neumann,[1],[2] F. Castro[1] A. Neumann[3] and M. Sbert[1]

[1] Institut d'Informàtica i Aplicacions. Grup de Gràfics de Girona (GGG). Universitat de Girona. Girona (Spain)
[2] Institució Catalana de Recerca i Estudis Avançats (ICREA) Barcelona (Spain)
[3] Institut fur ComputerGraphik und Algorithmen. TU Wien. Wien (Austria)

Abstract
In closed environments, especially in bright colored interiors, there occurs a significant change of saturation and some shifting of hue of originally selected colors. This is due to multiple light inter-reflections. The human vision mechanism partly reduces this effect thanks to the change of the reference white.

We use in this paper a multispectral radiosity method to describe and compute the physical effects. We also use a color appearance model, the new and powerful CIECAM02 model, to compute the perceptual aspects. The CIECAM02 includes the luminance and chromatic adaptation effects, and it has compact forward and inverse transformation formulas. The input data for the color appearance model is ensured by computing the radiosity solution, thereby there are known both the spectral radiance for every viewpoint and view direction and the spectral irradiance on every patch of the scene.

Nearly all of earlier global illumination approaches ignored the often strong changes of originally selected colors. This paper supports the color environment design. Using the presented method it is possible the selection or mixture of paints to achieve, after the physical and perceptual effects, a color appearance previously selected under standard viewing conditions in a color atlas.

1. Introduction

The color appearance problem has two components: the physical effects and the perceptual aspects. The physical model of the light interactions is described by the rendering equation [16,6] in general environments and by the radiosity equation [4,5] in diffuse environments. The more widely used approach uses only 3 color channels, that are generally enough for realistic rendering.

However, an accurate description of colors requires a multispectral approach [10]. These techniques use discrete spectral lines or a step-wise constant approach on the visible spectrum for all components of the model (from reflectivity to light sources). In a radiosity approach, the number of values needed for each patch is the number of these spectral intervals. On the other hand, the full spectrum models describe a lot of interesting phenomena missing in a simple RGB approach. There appear new characteristics, like e.g. the metamerism or the possibility of exact photometric luminance calculation based on spectral luminous efficiency of human eye.

After inter-reflection computation, the results can be significantly different between a simple RGB model and a multispectral one having the same starting tristimulus color coordinates (e.g. CIE XYZ) for all surfaces and light sources in the scene [10,11].

A drawback of the multispectral approach, especially in case of fine spectral resolution, is the high computational cost. This problem can be overcome by means of parallel computing. Another practical problem of the multispectral approach is often the lack of spectral data.

We deal in this paper with diffuse scenes (because of simplicity and speed), but the extension to non-diffuse environments, using one of the existing Monte Carlo methods [22] (like ray-tracing, Metropolis,etc.), is very easy. The novelty of the paper is not a new global illumination technique, but the combination of the multispectral global illumination with an accurate color appearance model to describe the color changes and to select the appropriate paint to invert or compensate the color changes.

To illustrate with a very simple case the color shifting let

us see a cube and a simple RGB model. Let all the bright colored walls have the same $(R, G, B) = (0.95, 0.90, 0.80)$ reflectivity values describing a highly unsaturated warm and bright color, having only some percent higher red than green component. Like in the ambient term calculations [19], we can obtain the result of multiple reflections in form of a geometrical series. Thus we obtained from original (R,G,B) after inter-reflection the $(R', G', B') = (19, 9, 4)$ in which is a highly saturated reddish-orange color, having over twice as large red than green component. This also results in a hue shifting.

We will also use in the paper very simple unoccluded radiosity model with 1-nm spectral resolution. The cube model with 6 unknowns and the more flexible brick model having already 'furnish factor' and window size (9 unknowns). These extremely simple approaches are often enough to describe the typical spectral color changes due to inter-reflections. We use of course complex radiosity models too, but with 10-nm resolution. This model requires 31 unknowns for each patch. We have to give data for all the surfaces and light characteristics with a set of 31 values.

The human vision system depending on viewing conditions will change the appearance of colors. Widely known fact is that we see a white paper as white in daylight and in tungsten light too, although this latter contains about 4 times more energy in the reddish range than a typical daylight. This is possible because of different nonlinear chromatic and luminance adaptation processes in retina and in the whole of the human vision system. A very interesting question and a central topic of our paper is, how will be reduced or compensated by the human vision the physical change of colors due to the multiple inter-reflections working like a natural 'saturation amplifier'. One of the problems to solve is to find colors with their spectral reflectance curves, which look in a color palette or in a color atlas in e.g. daylight perceptually equivalent to an interior after all physical and perceptual effects. We will find the best approximation from a given set of colors defined by their spectral reflectance from a color atlas.

It is more difficult to invert the problem in closed form: to find directly the spectral curves with the required properties. The more complex problem in this context is to find spectral reflectance curves, resulting in the same color appearance for a given set of possible lighting conditions: daylights with different color temperature and tungsten light and/or some of typical office lighting. We refer to this problem and demonstrate it with one case from our parallel research about perceptual metamerism.

2. Color Appearance Models

2.1. Principle of color appearance

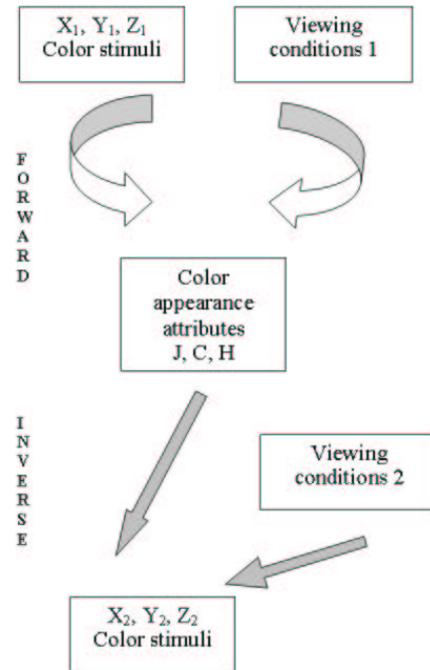The schema of the color appearance problem is illustrated by Figure 1

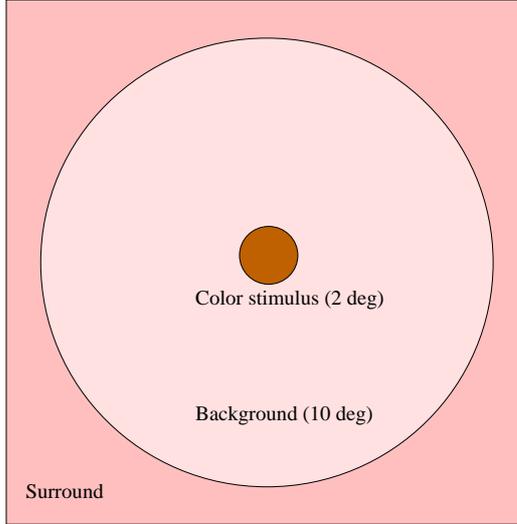**Figure 1:** *The color appearance problem.*

The core of all color appearance models is to find invariant color appearance attributes. Typically lightness, chroma and hue attributes, which ensure invariant color perception. We perceive the same color under different viewing conditions if the appearance attributes remains the same. We can compute these attributes of a given color observed under a given viewing condition. The inverse calculation means, that starting from these unchanged perceptual attributes having a new viewing condition we compute the appropriate new XYZ color stimuli. We will perceive both as equivalent, although e.g. in a printed version having the same viewing condition these colors look sometimes significantly different.

2.2. Viewing conditions

Fig. 2 shows the most important input factors of a color appearance model. The components of viewing field are:

- The observed color sample, the color stimulus is generally sub-tending roughly 2 degrees in the center of field of view.
- The background is roughly a 10 degree region immediately surrounding the stimulus. A useful guideline is that a thumb at arm's length is about 2 degree and the size of a clenched fist at arm's length is roughly 10 degrees.
- The surround is the field outside the background.

We do not use the so-called proximal field [2] which is an immediate environment of the stimulus extending for about

Figure 2: *The color appearance problem.*

2 degrees from the edge of the stimulus in each direction, to describe the simultaneous contrast or assimilation effect, because for big walls and surfaces it does not exist. Typically in our case also the background has identical properties than the stimulus.

For us the new CIECAM02 [14, 25, 23, 15] is an ideal color model. The CIE committee TC8-01 has recently published the CIECAM02 as a significant improvement and simplification of CIECAM97s [13, 12].

The detailed forward formulas of CIECAM02 color appearance model and a schema of inverse can be found in the Appendix.

2.3. Input color and luminance data

(X, Y, Z)	CIE XYZ color stimuli coordinates
(X_w, Y_w, Z_w)	Coordinates of adopted (or reference) white point
Y_b	CIE Y background coordinate
L_A	Absolute photopic luminance of adapting field (cd/m^2)
L_{Aw}	Absolute photopic luminance of reference white (cd/m^2)

Table 1: *Input color and luminance data.*

Some example data can be found for CIECAM02 model in [25]. We illustrate our example using Fig. 3. Let us assume

an "Average" viewing condition (see. Appendix, Table 5), and a medium gray background with $Y_b = 18$ for all 3 cases. The reference white is first a Planck radiator of T = 7500 K, one which is slightly bluish. The color stimuli coordinates (Table 1) are in this first case (X,Y,Z)= (61.34, 59.94, 50.07), a pastel color with orangish hue. After the forward color appearance calculation we obtain the J= 81.59, C= 21.56, h= 59.40 color appearance attributes. To ensure the same color appearance this values have to remain invariant under the changed viewing condition. Table 2 shows the new (X_w, Y_w, Z_w) reference white values, the new L_A luminance values of adapting field in cd/m^2 and the new X, Y, Z color stimulus having the same (J, C, h) triplet. The pictures do not demonstrate the real viewing conditions with a gray background, but show according to Table 2 the reference white colors and in the middle part the changed color stimuli. This will be corrected by human vision for the same appearance. Note that the change is significant (Table 2) but after multiple inter-reflections the earlier ignored changes in global illumination techniques are often more significant.

| $T(K)$	**7500**	**6000**	**4500**
L_A	954.93	636.62	318.31
X_w	87.12	87.38	89.32
Y_w	90.00	90.00	90.00
Z_w	112.95	93.91	68.24
X	61.34	62.58	65.42
Y	59.94	60.41	61.10
Z	50.07	41.62	30.24

Table 2: *Same color appearance with different white points.* $(J = 81.59, C = 21.56, h = 59.40)$

2.4. Background and Surround Luminances

To compute the background data we can define the angular field around the view-axis. We can rotate by 1-degree and 11-degree in the direction of a line around the axis. The inner and outer cones will define the background. Let D_b be the set of directions in the double cone. To compute the *relative luminance* Y_b we have to average the directional Y values according equation (6):

$$Y_b = \frac{\int_{D_b} Y d\omega}{\int_{D_b} d\omega} \tag{1}$$

The denominator is the solid angle (in steradian) between both cones. We evaluate the value in (1) by Monte Carlo sampling in D_b and averaging the obtained samples. The
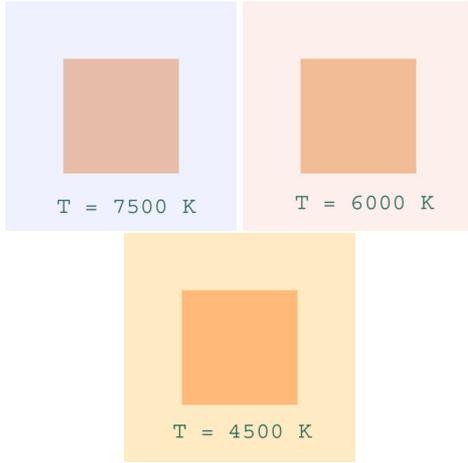
Figure 3: *Same color appearance with different white points (different temperature). (a) 7500 K. (b) 6000 K. (c) 4500 K.*

number of samples can be small because of the relative homogeneity of the wall color. Moreover, we can often use in the middle of a big wall, instead of (1), the *Y* of color sample as Y_b.

Monte Carlo sampling can be also used to compute L_A, the average absolute luminance of the surround. In this case the inner cone is defined by 11-degree and the outer cone is defined by 90-degree from axis, corresponding to the full hemisphere. In practice the exact shape of the outer cone is not the full hemisphere because of the structure of retina and some occlusion due to the shape of the human face around the eye. We will first describe in next chapter photometric and radiometric conversions. Knowing these conversions, the computations of *absolute luminance L_A* by the above-mentioned method are evident.

3. Photometric and radiometric quantities and conversions

3.1. Units

The radiosity method works with radiometric units at each color channel. Photometry uses different units. The reason of this fact it is not simply the different application area or the tradition, but the perceptual aspect: photometry depends on the human eye, especially on photopic spectral luminous efficiency $V(\lambda)$, that describes the wavelength-dependent sensibility of retina in the photopic range according CIE standard photometric observer (note that we just deal in this paper with the photopic range, in which we can perceive the colors by the retina cones, and not with the scotopic range, that corresponds to perception in dark, that is, under a given luminance level). Table 3 summarizes the different radiometric and photometric magnitudes and units.

Description	Radiometric magnitude	Radiom. unit	Photometric magnitude	Photom. unit
Energy	Energy	joule (J)	Luminous energy	*lumen sec*
Power	Radiant power (radiant flux)	watt (W)	Luminous power (luminous flux)	*lumen(lm)*
Intensity from a point source	Radiant intensity	$W sr^{-1}$	Luminous intensity	$candela(cd) = lumen\, sr^{-1}$
Power falling on surface	Irradiance (incoming radiosity)	$W m^{-2}$	Illuminance	$lux = lumen\, m^{-2}$
Elementary surface, given direction	Radiance	$W m^{-2} sr^{-1}$	Luminance	$cd\, m^{-2} = lux\, sr^{-1}$

Table 3: *Radiometric and photometric magnitudes and units.*

3.2. Photometric values from Radiometric data

The relation between radiometric and photometric magnitudes involves the wavelength λ of the light. We can express this relation in the following way:

$$683 * V(\lambda)\ lumen\ =\ 1\ Watt \tag{2}$$

where *V* is a function of λ that has its maximum value of 1 at 555*nm* (green region of the spectrum) and a value of only 0.1 at 429*nm* or 651*nm*, corresponding to blue and red regions of the spectrum, respectively (this means that, for instance, a $1/V(651) = 10[W]$ red lamp produces approximately the same luminance as an $1[W]$ green lamp). The shape of the luminous efficiency *V* is similar to the Gaussian curve. It is strictly positive only for the visible spectrum: $[360nm, 830nm]$, but in practice we can just consider the $[400, 700]$ interval, because the values of *V* at its endpoints are only 0.000396 and 0.004102 respectively.

Note that the conversion for irradiance and radiance is similar. If the spectral irradiance distribution is given for the full visible spectrum, we have to integrate on the different wavelengths to obtain the illuminance (E). In computer graphics we use a discrete approximation. If the irradiance (incoming radiosity) $B_{in}[W/m^2]$ is given in *N* different wavelengths, the illuminance (E) results:

$$E[lux] = 683 \sum_{i=1}^{N} B_{in}(\lambda_i) V(\lambda_i) \tag{3}$$

For an ideal white diffuse surface lighted with an illuminance $E[lux]$, the luminance $L[cd/m^2] = [lux/sr]$ in each direction of the half-space is given by:

$$L[cd/m^2] = \frac{E[lux]}{\pi[sr]} \qquad (4)$$

Some typical ambient luminance levels are:

- starlight: $10^{-3} cd/m^2$
- moonlight: $10^{-1} cd/m^2$
- indoor lighting: $100..300 cd/m^2$
- max. of CRT monitors: $100 cd/m^2$
- sunlight: $10000...40000 cd/m^2$

3.3. Spectral Radiometric Conversions

Some formulas have a special interest when using spectral data. Let $S(\lambda)$ be the spectral irradiance in $[W/m2]$ and let $\rho(\lambda), 0 < \rho(\lambda) < 1$ be the spectral reflectivity on an elementary surface. We can compute the normalization factor m using $\bar{x}(\lambda), \bar{y}(\lambda), \bar{z}(\lambda)$, the CIE 1931 color matching functions for 2 degree observation [2]:

$$m = \frac{100}{\sum_\lambda S(\lambda)\,\bar{y}(\lambda)} \qquad (5)$$

The CIE XYZ color coordinates of color reflected from the surface are then:

$$X = m \sum_\lambda \rho(\lambda)S(\lambda)\,\bar{x}(\lambda)$$
$$Y = m \sum_\lambda \rho(\lambda)S(\lambda)\,\bar{y}(\lambda)$$
$$Z = m \sum_\lambda \rho(\lambda)S(\lambda)\,\bar{z}(\lambda) \qquad (6)$$

For an ideal white diffuse surface, the relative luminance value Y will be 100. From a known irradiance, we can apply the formulas above to compute the color stimuli data. Similarly we can compute the Y of the background.

3.4. Direct Lighting and Color Temperature

Lighting is typically given in photometric units, like *lux*. For instance, noonday sun has an illuminance E = 100,000 lux or more, and a spectral distribution close to the standard CIE D65 source. A tungsten lamp can have illuminance values in 30..1000 lux, with a CIE standard A-light distribution (for reading, 200 lux are recommended) [7, 26].

The Plank distribution, that describes the ideal blackbody radiation at temperature T [Kelvin], is useful for a wide range of applications. The relative spectral distribution of a Planck radiator in a numerical stable form is given by the next equation

$$Planck(\lambda, T) = \left(\frac{1000}{\lambda}\right)^5 \left(e^{\frac{14387669}{\lambda T}} - 1\right)^{-1} \qquad (7)$$

Source	Color T [K]	Efficacy [lm/W]
North-sky light	7500	
Average daylight	6500	
Xenon flash	6500	
Sunlight + skylight	5500	
Sunlight 20° alt.	4700	
Sunlight 10° alt.	4000	
Fluorescent lamps (white or natural)	3500	
Tungsten halogen lamps (short life)	3300	
Studio tungsten lamps	3200	25
Fluorescent lamps (warm white)	3000	83
Tungsten halogen lamps (long life)	3000	21
Tungsten (100 W, 110 V)	2850	15
Tungsten (100 W, 240 V)	2750	13
Tungsten (40 W, 110 V)	2700	12
Tungsten (40 W, 240 V)	2650	10
Sunlight at sunset	2000	
Candle flame	1900	

Table 4: *Temperature and efficacy for different light sources.*

where λ is the wavelength in nanometer and T the temperature in Kelvin. We can approximate different spectral light distributions with the nearest appropriate Planckian distribution characterized by its temperature. This can define the color temperature of different light sources. The D65 standard CIE daylight has approximately T = 6504 K and CIE A-source similar to a tungsten light has approximately 2856 K color temperature. In Table 4 we present some useful color temperature data corresponding to different light sources [2]. We also present, in some cases, the efficacy [2] in lm/W, that represents . This efficacy values allow us to compute the photometric luminous power (in lumen) from the radiant power for some light sources. Note that, comparing to the constant in equation (2), the values of the efficacy are clearly lower. This is due, on one hand, to the fact that a big part of the energy corresponds to the poor range of $V(\lambda)$ (reddish region of the spectrum), and, on the other hand, to the energy dissipation of bulbs. Roughly 90 percent will be radiated in infrared range.

3.5. Spectral Irradiance

For tungsten or fluorescent lamps with known relative spectral distribution, efficacy, nominal power [W] and geometry we can compute the radiometric spectral irradiance values using formulas in 4.2. For other light sources we can measure the illuminance, or also we can use a recommended approximate value for illuminance and, using the Planck formula (7), the spectral irradiance can be calculated.

The spectral irradiance has a central importance in color appearance calculations. Starting from the solution of the radiosity problem we can easily calculate the irradiance or incoming radiosity $B_{in}[W/m2]$:

$$B_{in}(\lambda) = \frac{B_{out}(\lambda)}{\rho(\lambda)} \qquad (8)$$

The outgoing radiosity B_{out} is the classical 'radiosity' value, while B_{in}, the incoming radiosity, is equivalent to the irradiance at each wavelength. The reflectivity $\rho(\lambda)$ is always strictly positive for every λ according to real materials.

The irradiance calculation for different rendering techniques is described in [17], which deals with irradiance-based tone mapping, used widely in photography and movie industry.

The application of CIECAM02 color appearance model for each pixel is also a tone mapping method partly based on irradiance, unlike most of widely used tone mapping techniques, that use only view-depending radiance values [18]. However, the local gradient and other spatial vision effects will be not taken in consideration if we use CIECAM02 as tone mapping method, even using pixel-dependent background luminance.

3.6. The reference white

If the illumination is not homogenous, the reference white point is not a trivial question. In the radiosity context, patches near the corners have typically different colors from patches in the middle area of the walls. We can use an average value, namely a weighted average of white surfaces occurred in the surround. This weighted average gives a higher weight to the patches near the central view-axis. In case of mixed mode illumination having both daylight and tungsten lamps in view-field, the reference white is not an evident question, but we can use the above-mentioned method as a good approximation. We have to compute the L_{Aw} luminance in $[cd/m2]$. If we have only one reference white surface in the scene with reflectance curve $\rho_w(\lambda)$, and the incoming radiance B_{in}, obtained using equation (8), is constant over the white surface, we have

$$L_{Aw} = 683/\pi \sum_{\lambda} B_{in}(\lambda)\, \rho_w(\lambda)\, V(\lambda)) \quad [cd/m2] \qquad (9)$$

The L_{Aw} will be used for calculation of the surround factor (see Table 5 in the Appendix). To calculate the (X_w, Y_w, Z_w) coordinates of reference white we use the $\rho(\lambda) = \rho_w(\lambda)$, the $S(\lambda) = B_{in}(\lambda)$ spectral irradiance distribution in the formulas (6).

4. Photometric Radiosity

4.1. Multispectral Radiosity

Multispectral radiosity is given by Equation (10) using the classical notation in radiosity [4,5].

$$B_i(\lambda_k) = S_i(\lambda_k) + \rho_i(\lambda_k) \sum_j F_{ij} B_j(\lambda_k) \qquad k = 0, 1, ..., 30.$$

$$(10)$$

Note that here S_i is used for the self-emission $[W/m^2]$ (because the usual E is used for luminance in photometric context). On the other hand, $\lambda_k = 400 + 10k[nm]$, thus B_i, S_i, ρ_i are not characterized by a triplet, but by spectral functions.

In the complex radiosity environments used in this paper 3 different spectral reflectivity curves (Fig. 4) with different spectral light distributions are applied as wall colors.
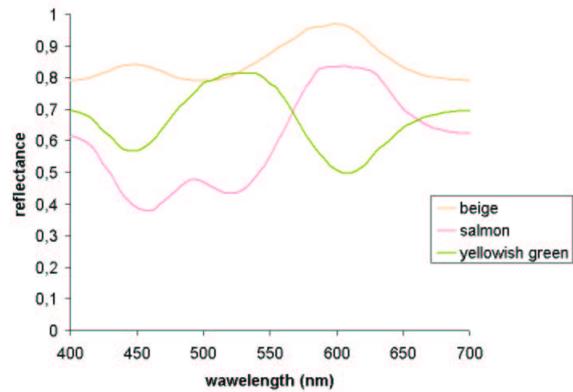
Figure 4: *Spectral reflectances of 3 wall colors.*

4.2. First Shot

We can calculate for sunlight or for an point source the secondary self-emission of direct-lighted patches in the following way. Let the luminance be $L[cd/m^2]$ as effect of the light source at the receiver patch. The calculation of L requires the knowledge of the light source, the cosine of the light incident on the patch and the distance in case of point sources. Let the relative (not-normalized) spectral distribution of light be $S^*(\lambda)$, e.g. D65, CIE-A, for daylight and tungsten light, or a Planckian one. Then, using 4, the illuminance is:

$$E \, [lux] = L \, \pi = c \, 683 \sum_{\lambda} S^*(\lambda) V(\lambda) \, [W/m2] \qquad (11)$$

In the formula (11) c is a free constant, and the secondary self-emission $S(\lambda)[W/m2]$ at wavelength λ can be computed (equation 10) using this constant c and reflectivity $\rho(\lambda)$:

$$S(\lambda) = \frac{E \, \rho(\lambda) \, S^*(\lambda)}{683 \sum_{\lambda} S^*(\lambda) V(\lambda)} \qquad [W/m2] \qquad (12)$$

4.3. The cube and the brick model

These simplified geometrical models apply 1nm high spectral resolution. The *cube model* is the simplest one in which we have calculated the multiple diffuse inter-reflection effect. This model includes just 6 patches, corresponding to the 6 sides of a cube. We can solve the corresponding radiosity system of equations in a closed form, working in this way with a high spectral resolution: 471 different values covering the full visible spectrum $[360nm, 830nm]$. The input data are, for every wavelength and patch, the reflectivity ρ_i and the self-illumination $S_i \, [W/m2]$. The form factors F_{ij} are approximately equal to 0.2 for each (i, j) pair (note that this is a very good approximation). The form factor F_{ii} is 0. Let also in this simple model the area A_j be equal to 1. The i-th row of the 6×6 matrix for a given λ is then

$$[-0.2\rho_i, -0.2\rho_i, ..., 1, ..., -0.2\rho_i] \qquad (13)$$

This simple problem can be solved in closed form

$$B_i = f(\rho_1, \rho_2, \rho_3, \rho_4, \rho_5, \rho_6) \qquad (14)$$

The spectral radiosity of observed wall i at each wavelength is a closed non-linear function of the spectral reflectance values of this wall i. This fact can be used in parametric inverse radiosity problem with pre-described spectral radiosity values. The closed form solution uses the B auxiliary term:

$$B = \sum_{i=1}^{6} B_i = \frac{\sum_{i=1}^{6} (1 + 0.2\rho_i)^{-1} S_i}{1 - 0.2 \sum_{i=1}^{6} (1 + 0.2\rho_i)^{-1} \rho_i} \qquad (15)$$

From B we compute the radiosity solution B_i:

$$B_i = (S_i + 0.2\rho_i B)(1 + 0.2\rho_i)^{-1}, \quad i = 1..6 \qquad (16)$$

A more flexible but simple possibility is the *brick model*. In this case we define the basis rectangle and the height of the room. One of the walls has a rectangular window with a given size. The lower part of the other 3 walls (from the floor level to a given percentage of height) has been assigned a different spectral reflectance, symbolizing the furniture-covered part. This represents a more correct result of the wall

color than in cube model, but also using a simple unoccluded environment.

In really complex scenes, the only cheap solution that gives an acceptable result is the *extended ambient term* [20]. This strategy does not use occlusion conditions, but only back-faces and quasi-shadows, for a radiosity-like approach.

4.4. Multispectral Radiosity for Complex Environments

For complex environments we can use different efficient radiosity techniques [8, 21, 9]. Practically all these methods can be parallelized when using more color channels. We will use 10 nm step in the $[400, 700]nm$ spectral interval. This means 31 color channels, that is, 31 unknowns for each patch. The light-source distribution also has to be defined using 31 values, similarly to the reflectivity curves of patches.

The evaluation of a given paint is described next. We compute the 31-channel radiosity solution. After this we select a typical patch e.g. in the middle part of a big wall, and we calculate the viewing condition parameters L_A, Y_b according chapter (2.4). From the spectral radiosity of the selected patch using (6) we can calculate the (X, Y, Z) color stimuli coordinates. The color of lighting will be determined by the incoming spectral irradiance according equation (8). The reference white also has this "irradiance color". We can use ideal white diffuser $\rho_w(\lambda) = 1$ or we can select an existing white surface in the scene with its real spectral distribution to calculate the spectral version of the reference white. Using (6) this spectral white as $S(\lambda)$ spectral light distribution, and $\rho(\lambda)$ reflectivity of the selected patch, we can compute the (X_w, Y_w, Z_w) white point. Using (9) we can calculate the absolute photopic luminance of reference white L_{Aw}. For the relative background luminance Y_b we can simply use the Y value of color stimuli if the light distribution of the wall is homogeneous. Having already all of data required according Table 1 we can calculate with the CIECAM02 forward model the (J, C, h) color appearance attributes.

On the other hand, we have the (J_0, C_0, h_0) color appearance attributes of the originally selected color that we wish to see after all physical and perceptual effects. To calculate this triplet we have used 2000 *lux* illuminance, that is $L_A = 636.32cd/m^2$ adaptation luminance level, grey background with $Y_b = 20$, and the standard $D65$ white point. The quality of the color selection will be characterized by the perceptual distance between (J_0, C_0, h_0) and (J, C, h). The CIECAM02 model ensures for us a good metric using Cartesian coordinates of (J, C, h) space, e.g. the $[J, a_C = C \cos(h), b_C = C \sin(h)]$. In this space the Euclidean distance is approximately equal to the perceptual color difference.

For a given set of wall colors we can sequentially compute this color difference after solving the appropriate radiosity problems with different possible wall colors. Note that the same lighting has to be used in each case. E.g. we will study

a typical daylight situation in an office, or a typical tungsten lighting with a given luminance level in a workplace.

Some wall colors are evidently bad. We can filter them in a pre-selection with a rough rejection process. E.g. for an pastel apricot color we would not select a dark-brown of same hue or just some color of significant different hue, like in range from purple until green. A possible radical pre-selection needs some further investigation.

5. Results
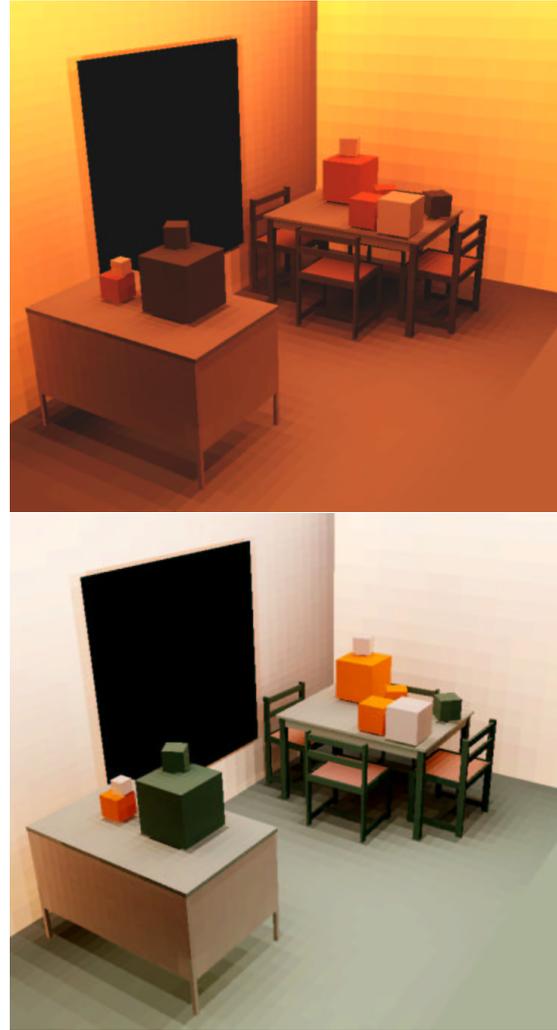
5.1. Effects of Interreflections

Figure 5 demonstrates the possible extreme effect of multiple interreflections. Using a multispectral radiosity model and a tungsten lighting we have received a reddish-orangish picture (top), reminisant of a photograph made with a daylight slide in a tungsten lighted environment. The human vision system is surprisingly able to invert this effect, as shown in the bottom image. Also in daylight environment it occurs a color shifting.

All of global illumination methods give bad results without the inversion effect obtained using an appropriate color appearance model. All of these problems are similar to using a flash in a bluish, greenish or cold yellowish interior, resulting in disturbing bad skin-colors. In radiosity or in non-diffuse global illumination sometimes the problem is not so disturbing, only because typically we do not have a priory expectations or cognitive color-knowledge, like in the case of skin colors.

The human observer is able, using the reference white, similar to digital photo and video cameras, but more in a more precise way, to invert the color changes. The key question is the referenced white, that is, the so-called 'adopted white point'. The most disturbing changes are easily convertible until an acceptable level, like in Figure 5.

Figure 6 shows, for 3 different colors (salmon, beige and yellowish green) the extreme high change in CIE *xy* chromacity diagram after multiple interreflection. The colors correspond to the graph 4 and to the first column of Figure 7. In the chromacity diagram (Fig. 6) the red lines illustrate the bigger change using tungsten lighting, and the shorter blue lines represent the smaller change using daylight. Figure 8 shows the color changes after interreflection and using the color appearance model. The a_c b_c are the Cartesian CIECAM02 coordinates: $C \cos(h), C \sin(h)$. The intersection points are the originally selected colors of Figure 7, and the free end points correspond to the changed perceptual attributes according second and third column in Figure 7.

We even use a color appearance model like the powerful CIECAM02 with its compact forward and inverse formulas, we do not receive as result the perceptual attributes of originally selected color because of nature of multispectral radiosity. The spectral reflectivity and light source curves

Figure 5: *Multispectral radiosity in tungsten light (top). Same picture according human vision using inverse color appearance model (bottom).*

and the final effect of interreflection are deeply non-linear processes. The color appearance models work with triplets and not with full spectra functions. All of these difficulties result in some cases strange, but in some cases acceptable color changes. Studying Figure 7, the first column shows salmon, beige and yellowish green colors according to spectral curves in Figure 4. We have studied the effect of tungsten and daylight in complex radiosity environment according to Figure 5. After the appearance calculations, which reduces the extreme shifting, similar to Figure 5 for beige color we have received a very high chroma decrease from 22 to 6 approximately, but the lightness is practically unchanged. For the first salmon color the chroma decrease only to half ap-
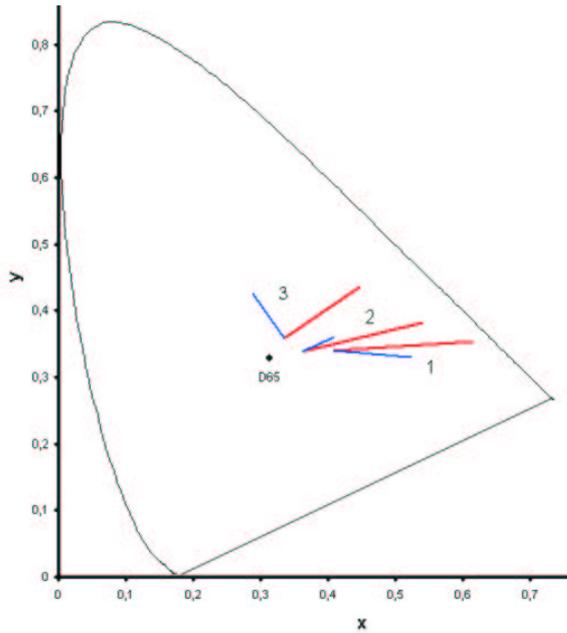
Figure 6: *Representation of x, y coordinates in case of (1) salmon, (2) beige and (3) yellowish green after interreflections in daylight (blue) and tungsten light (red).*

Figure 7: *Color appearance of 3 paints in a room lighted with tungsten and daylight.*

Figure 8: *Representation of a_c, b_c coordinates in case of (1) salmon, (2) beige and (3) yellowish green after interreflections in daylight (blue) and tungsten light (red).*

prox., while the third yellowish color had a one and a half chroma increasing. All of the 3 original colors had in final appearance also a significant hue change, the most disturbing is for the yellowish green, what in daylight from $H = 95Y$ $5G$ is changed to $H = 3Y$ $97G$. This nearly unbelievable after multiple checking was correct.

The authors earlier solved the perceptual metamerism problem without taking into consideration the multiple interreflection effects. Spectral curves in Figure 4 were planned for daylights D75, D65, D55 and CIE-A light sources. The method was able to ensure after color appearance the same perceptual attributes. This is perhaps the reason of the waves in the curves in Figure 4. We can also give an explanation for Figure 7, where the colors in tungsten and daylight situation are very similar, although being also involved in the question the multiple interreflections.
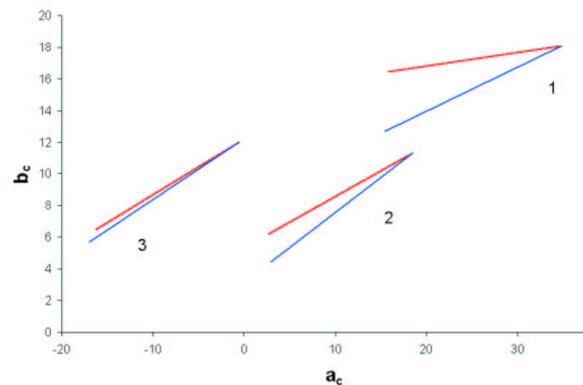
6. Conclusions and Future Work

One possible goal in color design of interiors is to receive a pre-selected color appearance after the physical and perceptual effects. The physical effects are the typical spectral changes due to the global illumination problem because of multiple light reflection.

Our results demonstrate the expected effects. The modified reference white is similar to a colored ambient light containing the effects of multiple light reflections. This ref-

erence white reduces the strong color changes in interiors. The problem of color change appears to be lower in dark environments and sometimes higher for bright interiors, especially in a range of saturation that depends on hue.

One of the future lines of research would consist on mapping the full gamut of solid colors, giving for some typical style of interiors a new appropriate color atlas containing the pigments -according to final color appearance- with their spectral reflectance curves.

Other future work consists of studying the possibility of analytical inversion of the multispectral radiosity for the

simplest cube or brick model where the solution is given in a closed form.

A real challenge consists of defining highly metamer reflectance curves, and thus perceptually highly stable colors under different lighting situation. Some industrial applications can be found in the fields of interior design, paint production, etc., motivating further research.

Acknowledgments

References

1. M.D. Fairchild. *Color Appearance Models*. Addison Wesley, 1998.

2. R.W.G. Hunt. *Measuring Color*. Ellis Horwood Ltd., 1992.

3. A. Nemcsics. *Color Dynamics, Environmental Color Design*. Ellis Horwood Ltd., 1993.

4. F.X. Sillion and C. Puech. *Radiosity and Global Illumination*. Morgan Kaufmann Publishers Inc., 1994.

5. M. Cohen and J. Wallace. *Radiosity and Realistic Image Synthesis*. Academic Press Professional., 1993.

6. A.S. Glassner. *Principles of Digital Image Synthesis*. Morgan Kaufmann Publishers., 1995.

7. G. Wyszecki and W.S. Stiles. *Color Science*. Wiley, 1982.

8. M. Sbert. *The Use of Global Random Directions to Compute Radiosity. Global Monte Carlo Methods*. Ph.D. thesis, UPC, 1997.

9. P. Bekaert. *Hierarchical and Stochastic Algorithms for Radiosity*. Ph.D. thesis, KU Leuven, 1999.

10. F.D. Yinlong Sun, M.S. Fracchia, T.W. Drew and A. Calvert. A Spectrally Based Framework for Realistic Image Synthesis. *The Visual Computer*, **17**:429–444, 2001.

11. G.M. Johnson and M.D. Fairchild. Full-Spectral Color Calculations in Realistic Image Synthesis. *IEEE Computer Graphics and Applications*, **19**(4):47–53, 1999.

12. N. Moroney. Usage guidelines for CIECAM97s. *Proc. IST PICS 2000 Conference*, 164-168, 2000.

13. N. Moroney. A comparison of CIELAB and CIECAM97s. *Proc. IST/SID 6th Color Imaging Conference*, 17-21, 1998.

14. N. Moroney, M.D. Fairchild, R.W.G. Hunt, C. Li, M.R. Luo and T. Newman. The CIECAM02 Color Appearance Model. *10th IST/SID Color Imaging Conference*, 2002.

15. C. Li, M.D. Fairchild, R.W.G. Hunt, M.R. Luo, N. Moroney and T. Newman. The Performance of CIECAM02. *10th IST/SID Color Imaging Conference*, 2002.

16. J.T. Kajiya. The rendering equation. *Computer Graphics Proceedings, Siggraph'86*, 143-150 1986.

17. K. Matkovic, L. Neumann and W. Purgathofer. A Survey of Tone Mapping Techniques *Spring Conference on Computer Graphics'97, Budmerice, Slovak*, 1997.

18. L. Neumann, K. Matkovic, A. Neumann and W. Purgathofer. Incident Light Metering in Computer Graphics. *Computer Graphics Forum*, **18** (4) 235-247 1998.

19. L. Neumann and A. Neumann. Radiosity and Hybrid Methods. *ACM Transactions on Graphics*, **14** (3) 233-265 1995.

20. F. Castro, L. Neumann and M.Sbert. Extended Ambient Term *ACM Journal of Graphic Tools*, **5** (4) 1-7 2000.

21. P.Bekaert, L. Neumann, A. Neumann, M. Sbert and Y.D. Willems. Hierarchical Monte Carlo Radiosity. *Rendering Techniques*, 259-268 1998.

22. P.Bekaert, M. Sbert and J. Halton. Accelerating path tracing by reusing paths. *Rendering Techniques (Eurographics Workshop on Rendering)*, 125-134 1998.

23. N. Moroney. Private Communication. 2003.

24. CIECAM02 *www.colour.org/tc8-01/*,

25. Examples for CIECAM02 model   . *www.cis.rit.edu/fairchild/CAM.html*,

26. Munsell Color Science Laboratori   . *www.cis.rit.edu/research/mcsl/online/cie.shtml*,

7. Appendix

This Appendix can be used by the reader without deeper color theory background, only using the presented formulas. [1] is useful to understand the real perceptual process.

To illustrate the importance of *CIECAM*02 model, we would first cite the Biography from the original paper [14] used in this Appendix:

"The authors of this paper have a combined 125 plus years experience in color science. They include chairs of TC1-3 that prepared *CIE* publication 15.2, TC1-34 that developed the *CIECAM*97s model and TC1-52 that over-viewed the development of chromatic adaptation transforms. The authors span eight time zones, two academic institutions and two corporations."

However, this is still an evolving topic, and it was originally designed for some imaging device. Thereby e.g. in computation of surround factor below, we need some additional ideas.

7.1. Viewing Condition Parameters

We can use as rough approximation e.g. "dim" surround if overall illumination is lower than 40 lux (but not dark), "average" if it is over 40 lux. But using equation (17) is a better approach [23].

Having the absolute luminances of surround and of the reference white we compute the surround factor:

$$Surround\, factor = \frac{L_A}{L_{Aw}} \qquad (17)$$

Using Table 5 we have the F, c and N_c factors. For intermediate surrounds, the values in Table 5 can be linearly interpolated.

Table 5: *Viewing condition parameters for different surrounds.*

Surround factor	F	c	N_c
1.0 (Average)	1.0	0.69	1.0
0.2 (Dim)	0.9	0.59	0.95
0.0 (Dark)	0.8	0.525	0.8

Using the luminance L_A (cd/m^2) of adapting field and the term $L = 5L_A$, we can compute the factor F_L using the following notation:

$$k = (L+1)^{-4} \qquad (18)$$

Thus $\qquad F_L = 0.1 * [2kL + (1-k)^2 L^{\frac{1}{3}}] \qquad (19)$

n is a function of the luminance factor of the background and of the adopted white point:

$$n = \frac{Y_b}{Y_w} \qquad (20)$$

Thus this value can be used to compute the chromatic and brightness background induction factors N_{bb} and N_{cb}, and also z as seen in next equations:

$$N_{bb} = N_{cb} = 0.725n^{-0.2} \qquad (21)$$

$$z = 1.48 + \sqrt{n} \qquad (22)$$

Note that this corresponds to the computation of several of the perceptual attribute correlates.

7.2. Chromatic adaptation

From (X,Y,Z) color stimuli or (X_w, Y_w, Z_w) white point we can compute the appropriate linear (R,G,B) and (R_w, G_w, B_w) triplets using the *CAT*02 matrix:

$$\begin{bmatrix} R \\ G \\ B \end{bmatrix} = \begin{bmatrix} 0.7328 & 0.4296 & -0.1624 \\ -0.7036 & 1.6975 & 0.0061 \\ 0.0030 & 0.0136 & 0.9834 \end{bmatrix} \begin{bmatrix} X \\ Y \\ Z \end{bmatrix} \qquad (23)$$

The D factor or degree of adaptation will be computed from luminance adaptation level L_A and from factor F depending on viewing condition (see Table 5)

$$D = F[1 - \frac{1}{3.6}e^{-\frac{L_A+42}{92}}] \qquad (24)$$

Having (R,G,B) from (23) and D from (24) the full chromatic adaptation transform can be written as

$$R_c = [\frac{Y_w}{R_w}D + (1-D)]R \qquad (25)$$

for red channel (G_c and B_c can be calculated by a similar manner, and so R_{cw}, G_{cw}, B_{cw}). Subscripts w denotes the corresponding values for the white point. Note that equation (25) includes the factor Y_w. This means that the adaptation is independent of the luminance factor of the adopted white point. For instance, a reflection print could have a Y_w of less than 100, say equal to 90. Such a print under an equi-energy illuminant would have values of X_w, Y_w, Z_w and R_w, G_w, B_w all equal to 90. In this case R_c, G_c, B_c will be equal to $(D/9+1)R, (D/9+1)G, (D/9+1)B$. But, because the equi-energy illuminant is being used, there is no chromatic adaptation, and R_c, G_c, B_c should be equal to R, G, B. Multiplication by Y_w ensures that the adaptation is independent of the luminance factor of the adopted white point.

The R_c, G_c, B_c values are then converted to *Hunt-Pointer-Estevez* (HPE) space before the post-adaptation non-linear response compression is applied. Using the product of *HPE*

and inverse *CAT*02 matrices we obtained the (R', G', B') triplet in the *HPE* space:

$$\begin{bmatrix} R' \\ G' \\ B' \end{bmatrix} = M_{HPE} M_{CAT02}^{-1} \begin{bmatrix} R_c \\ G_c \\ B_c \end{bmatrix} =$$

$$\begin{bmatrix} 0.740979 & 0.218025 & 0.0410003 \\ 0.285353 & 0.624201 & 0.0904487 \\ -0.009628 & -0.005698 & 1.015400 \end{bmatrix} \begin{bmatrix} R_c \\ G_c \\ B_c \end{bmatrix} \quad (26)$$

7.3. Non-linear response compression

The *post-adaptation non-linear response compression* is then applied to the output of equation (26). The *CIECAM*02 non-linearity converges to a finite value for increasingly large intensities and it has a gradual toe for increasingly small intensities. Let functions f and g be:

$$f(x) = \left(\frac{F_L |x|}{100}\right)^{0.42} \quad (27)$$

$$g(x) = 0.1 + \frac{400 f(x)}{27.13 + f(x)} \quad (28)$$

The post-adapted responses are:

$$R'_a = g(R') \quad G'_a = g(G') \quad B'_a = g(B') \quad (29)$$

Note that for negative R', G' or B', R'_a, G'_a or B'_a, respectively, must be made negative.

7.4. Perceptual attribute correlates

Preliminary Cartesian coordinates a and b, are computed from equation (29):

$$a = R'_a - \frac{12}{11} G'_a + \frac{1}{11} B'_a \quad (30)$$

$$b = \frac{R'_a + G'_a - 2B'_a}{9} \quad (31)$$

A hue angle h in ($[0, 360]$) interval (in degrees) and an eccentricity factor e are computed from a and b in the following way:

$$h = \frac{180}{\pi} tan^{-1}(b/a), \quad if(h < 0) \quad h = h + 360 \quad (32)$$

$$e = N_c N_{cb} \frac{12500}{13}[3.8 + cos(h\frac{\pi}{180} + 2)] \quad (33)$$

The factor t:

$$t = \frac{e(a^2 + b^2)^{1/2}}{R'_a + G'_a + 1.05 B'_a} \quad (34)$$

The achromatic response A can then be computed:

$$A = N_{bb}(2R'_a + G'_a + 0.05B'_a - 0.305) \quad (35)$$

We compute the *A for the color stimuli and simultaneously A_w for the white point*. This means that the calculations shown in equations (23) .. (35) must be performed once for the (X, Y, Z) color stimuli and once for the (X_w, Y_w, Z_w) white point. From A and A_w we can compute the lightness J:

$$J = 100(\frac{A}{A_w})^{cz} \quad (36)$$

where c can be obtained from Table 5 and z can be obtained from equation (22). Having j, the factor t (from equation (34)) and n from equation (20), the chroma C can be computed:

$$C = 0.1 \, t^{0.9} \sqrt{J}(1.64 - 0.29^n)^{0.73} \quad (37)$$

7.5. Inverse Model

We will just use (J, C, h) triplet to inverse model calculations. The *CIECAM*02 description [14] contain the hue-quadrature, H, being a monotone function of h using the values of unique hues. H is not necessary for the inverse model, similarly to the Q (brightness), M (colorfulness), s (saturation) or the different Cartesian coordinates: a_C, b_C, a_M, b_M, and a_s, b_s.

The detailed description of inverse model will be published by *CIE* committee TC 8-01 [24]. First we compute, according the new viewing condition, the $F, c, N_c, F_L, n, N_{cb}, N_{bb}$ and z factors, and then we can compute with the new reference white the equations (23)..(35). So we have the A_w value. Starting from (J, C, h) we can calculate factor t, e and A (having A_w according to the new viewing condition). From t, e, A, h, we can calculate a 3-unknown linear equation system for the post-adapted non-linear R'_a, G'_a, B'_a values. Having this ones, the inversion is evident sequentially using the inverse of equations (29)..(23).